*J. Fluid Mech.* (1989), *vol.* 205, *pp.* 341–358
*Printed in Great Britain*



# Generation of large-scale structures in three-dimensional flow lacking parity-invariance

By P. L. SULEM[1,2], Z. S. SHE[1,3], H. SCHOLL[1,4] AND U. FRISCH[1]

[1] CNRS, Observatoire de Nice, BP 139, 06003 Nice Cedex, France
[2] School of Mathematical Sciences, Tel Aviv University, Israel
[3] Applied Computational Mathematics, Princeton University, NJ 08544, USA
[4] Astronomisches Rechen-Institut, Heidelberg, FRG

(Received 20 June 1988 and in revised form 21 February 1989)

The existence of an inverse cascade is demonstrated for three-dimensional incompressible flow displaying the Anisotropic Kinetic Alpha (AKA) instability (Frisch, She & Sulem). By means of full three-dimensional simulations of the Navier–Stokes equations, it is shown that flow stirred at small scales by an anisotropic force lacking parity-invariance (i.e. lacking any centre of symmetry) can generate strongly helical structures on larger scales. When there is a substantial range of linearly unstable modes, the most unstable ones emerge at first, but are eventually dominated by modes with the smallest wavenumbers.

The key observation for the theory of this inverse cascade is that, in the presence of forcing, the small-scale Reynolds stresses will become dependent on the large-scale flow. Elimination of the small scales produces the nonlinear AKA equations for the large-scale flow. The latter have non-trivial one-dimensional solutions also displaying an inverse cascade, qualitatively similar to the one reported above. This cascade has been numerically simulated over a range of more than two decades. For a simple choice of the forcing, a steady state is eventually reached; it can be described analytically and presents interesting geometric features in the limit of very extended systems. The corresponding energy spectrum has a $k^{-4}$ range. A number of other scaling relations are also derived.

The multi-dimensional extension of the theory is briefly considered. The resulting large-scale structures are conjectured to correspond to solutions of the incompressible Euler equation.

## 1. Introduction

It has been well established from considerable experimental and observational evidence that self-organization of flow into large structures is not precluded by turbulence and strong nonlinearities. There are instances where large-scale structures are produced by an instability acting directly at such scales. Here, we shall be interested in the alternative scenario where large-scale structures are produced by an inverse cascade. By this we understand that large structures are eventually emerging, although initially the instability acts dominantly at much smaller scales. Kraichnan (1967, 1976) suggested that the formation of large-scale structures in two-dimensional incompressible turbulence is due to an inverse cascade driven by

negative viscosity instabilities. The Kolmogorov flow near threshold has been shown to produce an inverse cascade (She 1987), which can be described in deterministic terms. In three-dimensional magnetohydrodynamics the inverse cascade of magnetic helicity has been related to the $\alpha$-effect instability (Frisch *et al.* 1975).

It has been found recently that three-dimensional (non-conducting) flow can also exhibit an instability, called the Anisotropic Kinetic Alpha (AKA) instability, when it is stirred at small scales by a force which combines anisotropy with lack of parity-invariance, i.e. no centre of symmetry (Frisch, She & Sulem 1987). We shall show here that this can lead to large-scale self-organization. We shall mostly consider an instance of the problem, which allows considerable analytic insight. In §2, we summarize basic general properties of the AKA effect; a more formal presentation together with some background material may be found in Frisch *et al.* (1987). In section §3, we give numerical evidence that the AKA effect may give rise to a generalized form of inverse cascade; this is based on a fully resolved three-dimensional simulation of the Navier–Stokes equations. In §4, we show that insight into this inverse cascade can be obtained from a one-dimensional model. Its numerical integration indeed reveals a very extensive inverse cascade, leading eventually to the formation of steady large-scale structures. Section 5 is devoted to the scaling laws of such structures in the limit of very large systems.

## 2. The AKA effect

We are interested in the effect of a large-scale velocity field superimposed on a flow governed by the incompressible Navier–Stokes equations, in a situation where the Galilean invariance is broken by stirring forces (or by boundaries). The Reynolds stresses can then become dependent on the large-scale velocity. If this happens, we shall say that there is an AKA effect. This, in turn, will affect the large-scale dynamics. Specifically, we assume a stirring force $\boldsymbol{f}(\boldsymbol{r},t)$, which is either periodic in space and time, or random homogeneous and stationary; we denote by $l_0$ its characteristic spatial scale. We assume

$$\langle f \rangle = 0, \tag{2.1}$$

where the angular brackets denote space–time (or ensemble) averaging. In the presence of a large-scale velocity $\boldsymbol{w}$, the resulting small-scale flow $\tilde{\boldsymbol{u}}$ satisfies the Navier–Stokes equations with an additional advection term:

$$\partial_t \tilde{u}_i + w_j \partial_j \tilde{u}_i + \partial_j(\tilde{u}_i \tilde{u}_j) = -\partial_i \tilde{p} + \nu \nabla^2 \tilde{u}_i + f_i, \quad \partial_j \tilde{u}_j = 0, \tag{2.2}$$

where, to leading order, $\boldsymbol{w}$ should be uniform and constant. The large-scale flow is governed by the AKA equation:

$$\partial_t w_i + \partial_j(w_i w_j + R_{ij}) = -\partial_i p + \nu \nabla^2 w_i, \quad \partial_j w_j = 0, \tag{2.3}$$

where the Reynolds stresses,

$$R_{ij} = \langle \tilde{u}_i \tilde{u}_j \rangle, \tag{2.4}$$

are $\boldsymbol{w}$-dependent through (2.2).

When the issue is the stability of the small-scale flow to weak large-scale perturbations, (2.3) can be linearized, yielding the linear AKA equation:

$$\partial_t w_i = \alpha_{ijl} \partial_j w_l - \partial_i p + \nu \nabla^2 w_i, \tag{2.5}$$

with

$$\alpha_{ijl} = -\left[\frac{\partial \langle \tilde{u}_i \tilde{u}_j \rangle}{\partial w_l}\right]_{w=0}. \tag{2.6}$$

The linear dependency of the Reynolds stresses on the large-scale flow directly (and not on space derivatives such as rotation or shear) is characteristic of the AKA effect.

We shall be here interested in situations lacking parity-invariance. Parity-invariance means invariance under space, velocity, and force reversals. As immediately follows from (2.6), parity-invariance implies that $R_{ij}$ is an even function of $\boldsymbol{w}$, and thus the vanishing of the $\alpha_{ijl}$ tensor. Note that helical flows necessarily lack parity-invariance, the converse being false. Similarly, the $\alpha_{ijl}$ tensor vanishes in isotropic situations, since the tensor is by construction symmetric in $i$ and $j$, and there exist no non-vanishing third-order tensors with such symmetry. Other instances of vanishing are given in Frisch *et al.* (1987) where a more systematic multi-scale derivation of the AKA-equations ((2.5)–(2.6)) is given. The scale separation between the basic flow induced by the forcing and the AKA-driven large-scale flow requires either a small Reynolds number, a small anisotropy or a small parity violation.

It is important to point out that (2.5) for the linear AKA effect may already be found in Krause & Rüdinger (1974). Our tensor $\alpha_{ijl}$ is there denoted $\Lambda_{ijk}$. However, Krause & Rüdinger restricted their investigation to homogeneous isotropic turbulence, so that the AKA effect disappears entirely. They also claim (in a note added in proof) that the effect disappears in homogeneous turbulence, a statement which is clearly too general.

For non-vanishing $\alpha_{ijl}$ tensor, the large-scale behaviour will depend on the eigenvalues of the operator in the right-hand side of the linear AKA equation (2.5). In two dimensions, it may be shown, using a stream-function representation, that the first-order operators produce only dispersive effects. Thus, large-scale weak perturbations will propagate, while being slowly damped by viscosity. In three dimensions, large-scale instabilities have been obtained, leading to exponentially growing helical modes (Frisch *et al.* 1987).

When instability occurs, it follows from (2.5), that the growth rate has the form $\alpha k - \nu k^2$, where $k$ is the wavenumber of the perturbation and $\alpha$ denotes a positive coefficient depending on the direction of the wavevector. This functional form of the growth rate is similar to that found for the $\alpha$-effect in MHD (Steenbeck, Krause & Rädler 1966; Moffatt 1978) and in compressible flows (Moiseev *et al.* 1983).

## 3. AKA instability and inverse cascade

The $\alpha$-effect is the main motor of an inverse cascade in three-dimensional MHD (Frisch *et al.* 1975; Meneguzzi, Frisch & Pouquet 1981). Brissaud *et al.* (1973) raised the possibility of an inverse cascade in ordinary incompressible three-dimensional helical flows. This effect could not be obtained in the context of isotropic closure calculations (André & Lesieur 1977). It is however conceivable that the AKA instability drives some kind of inverse cascade in anisotropic flows when there is a wide range of linearly unstable modes. If it exists, the phenomenon will manifest itself by the eventual dominance of the largest available scales. Note that such a cascade cannot result just from the linear AKA instability, since this would forever give dominance to the mode with the largest growth rate.

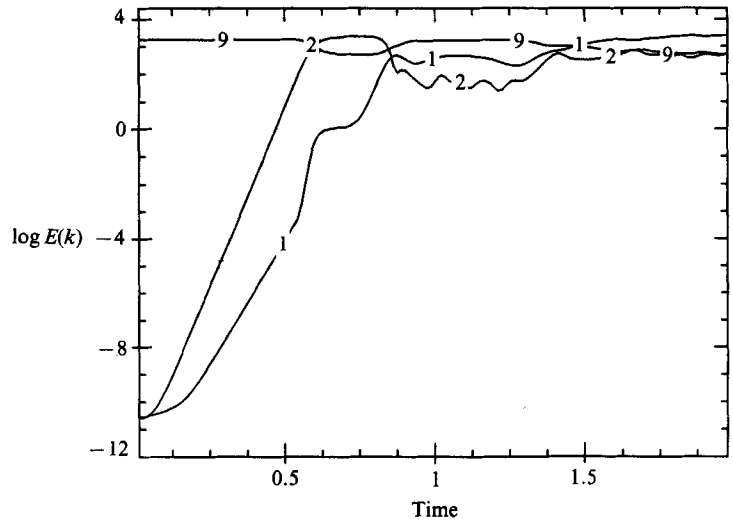


FIGURE 1. Fully resolved simulation of an AKA-driven inverse cascade using $32^3$ modes. The forcing is at wavenumber 9. The range of linearly unstable modes extends from wavenumbers 1 to 4. The evolution of the energy in modes of wavenumbers 1, 2, and 9 (as labelled) is shown in lin–log coordinates.

Henceforth, we shall be more specific and concentrate on the model of forcing used by Frisch *et al.* (1987), namely

$$\left.\begin{aligned} f_1 &= \frac{\nu V_0 \sqrt{2}}{l_0^2} \cos\left(\frac{y}{l_0} + \frac{\nu t}{l_0^2}\right), \\ f_2 &= \frac{\nu V_0 \sqrt{2}}{l_0^2} \cos\left(\frac{x}{l_0} - \frac{\nu t}{l_0^2}\right), \\ f_3 &= f_1 + f_2, \end{aligned}\right\} \tag{3.1}$$

where $V_0$ is a typical velocity from which we define a Reynolds number, characteristic of the small-scale flow:

$$R = \frac{V_0 l_0}{\nu}. \tag{3.2}$$

This is one of the simplest models which displays an AKA instability. Note that parity-invariance is broken by the time dependence. The time dependence can be removed by a Galilean transformation. However, it then becomes necessary to endow the basic flow with a uniform component. This somewhat blurs the distinction between large and small scales.

In order to test the possibility of an AKA-driven inverse cascade, we have set up various numerical experiments, two of which are now reported. The three-dimensional Navier–Stokes equations with the above forcing have been integrated by a spectral method. For an overall $2\pi$-space periodicity, the relevant parameters are the wavenumber $k_0 = 1/l_0$ of the small-scale forcing and the Reynolds number $R$. The unit of time is set by the choice $\nu = \pi$. In all the runs, a very low amplitude random seed, identical for all Fourier modes is introduced at time $t = 0$ in order to allow the development of large-scale instabilities.

The first experiment, performed at a resolution $32^3$, corresponds to $k_0 = 9$ and $R = 1.5$. Modes with wavenumber from 1 to 4 are linearly unstable, the maximum growth rate being reached for wavenumber 2. Figure 1 gives the time dependence of the energy $E(t, k)$ in spherical shells containing all the Fourier modes with

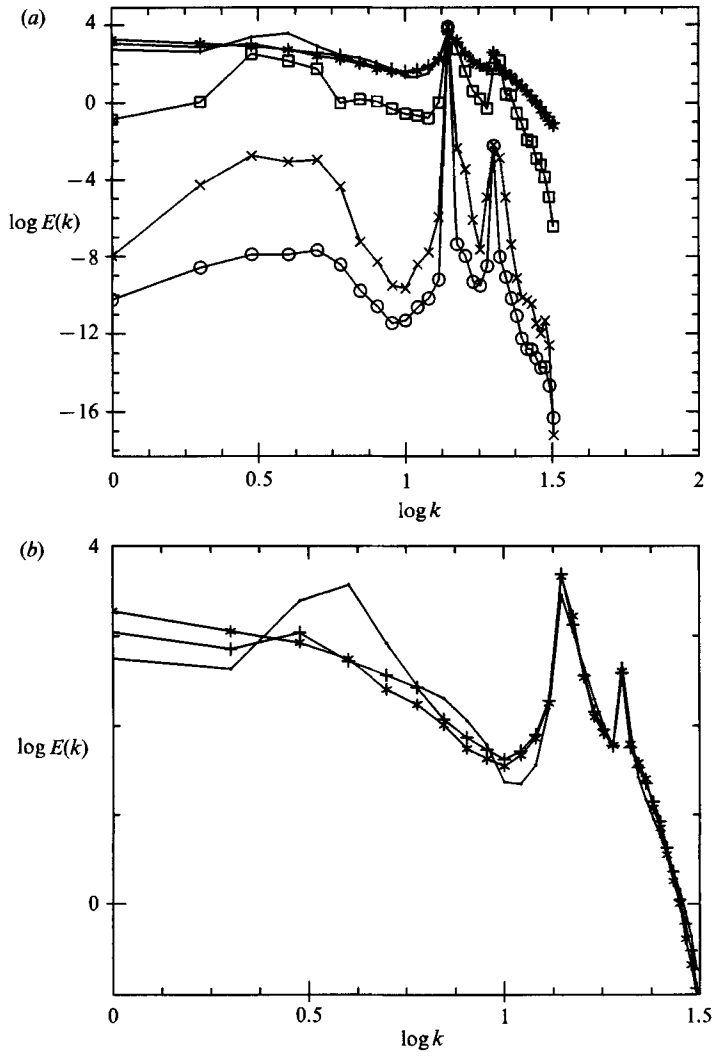


FIGURE 2. Fully resolved simulation of an AKA-driven inverse cascade, using $64^3$ modes. The range of linearly unstable modes extends from $k = 1$ to $k = 8$. Forcing is at wavenumber 14. The figure shows the energy spectrum $E(t, k)$ for various times in log–log coordinates. In (*a*), the dots are for $t = 0.05$, the plus signs for $t = 0.1$, the stars for $t = 0.15$, the circles for $t = 0.2$, the crosses for $t = 0.3$, and the squares for $t = 0.4$. For clarity, late times are shown enlarged in (*b*); the dots are now for $t = 0.2$, the plus signs for $t = 0.3$, and the stars for $t = 0.4$.

wavenumber from $k-1$ to $k$; for clarity, we display only $k = 1$, $k = 2$, and $k = 9$. Up to about $t = 0.5$, we obtain exponential growth for $k = 1$ and $k = 2$, the latter being much faster, as predicted by linear theory. Beyond this time, nonlinear effects become significant. We then observe at first a plateau, indicative of some kind of feed-back saturation (Frisch *et al.* 1987). Then, we find that the $k = 1$ modes leap-frog the $k = 2$ modes, around $t = 0.9$. Eventually, an approximately steady state is reached, with the modes of largest scale (smallest wavenumber) significantly dominant.

To find if this trend persists with a more extended range of unstable modes, we performed a second experiment with a resolution $64^3$. The forcing wavenumber is $k_0 = 14$ and the Reynolds number $R = 2$. The linearly most unstable modes are now around $k = 4$. With such a wider unstable range, it is of interest to show the evolution

of the full energy spectrum $E(t, k)$. Figures 2(*a*) and 2(*b*) display $E(t, k)$ for various early and late times, respectively. Until about $t = 0.12$, the fastest growing modes stay around $k = 4$, as expected from linear theory. Then, the dominant growth rate shifts to $k = 1$. Around $t = 0.2$, the linearly most unstable modes start depleting. At $t = 0.3$, the energy spectrum has its maximum at $k = 1$. At $t = 0.4$, an essentially steady state is reached in which the energy spectrum is decreasing for $k$ from 1 to 10. We refer to this dynamics as an inverse cascade. It is clearly not a step-by-step cascade of the Richardson type but rather a highly non-local process.

We have also analysed the flow in more detail by listing at various times the wavevectors of those large-scale modes contributing significantly to the energy spectrum. Up to about $t = 0.2$, only $z$-dependent large-scale modes are significant. Then, $x$- and $y$-dependent modes become appreciable, but never very strong; at $t = 0.4$. large-scale modes which are only $z$-dependent dominate, in energy, by about a factor four over other modes.

The preceding numerical experiments (which required several hours of CRAY-2) give some evidence that the AKA instability can drive an inverse cascade. At this point, however, it is not clear that the trend observed so far will persist with an even wider range of unstable modes. Pushing our full three-dimensional Navier–Stokes calculations much further would become impractical. A contracted description taking advantage of the separation of scales will allow us to proceed.

## 4. The one-dimensional nonlinear AKA equation

The AKA equation (2.3) can be used as a starting point for studying the large-scale dynamics, provided there is a separation of scales between the forcing modes and the unstable modes. This can be achieved in several ways. One way is to have a small Reynolds number $R$, defined by (3.2); the unstable modes then have scales $O(R^{-2})$ (in units of $l_0$), as shown by Frisch *et al.* (1987). Another way is to use a force with a weak violation of either parity or isotropy: this will make the $\alpha_{ijl}$ tensor (equation (2.6)) small, thereby ensuring the separation of scales. Finally, the separation of scales can be a dynamical consequence of the inverse cascade, when the latter has proceeded sufficiently far. Henceforth, separation of scales is assumed.

In order to use the AKA equation (2.3) effectively, we must be able to estimate the dependence of the small-scale Reynolds stresses $R_{ij}$ on the large-scale flow $\boldsymbol{w}$. For this, (2.2) must be solved, at least approximately. When the Reynolds number $R$ is small, (2.2) can be solved, to leading order, by dropping the nonlinear term $\partial_j(\tilde{u}_i \tilde{u}_j)$. For the specific example of stirring force (3.1), the Reynolds stresses are given, to leading order in $R$, by Frisch *et al.* (1987):

$$\left.\begin{aligned} R_{11} &= \frac{V_0^2}{2 + (2l_0/\nu)\, w_2 + ((l_0/\nu)\, w_2)^2}, \\ R_{22} &= \frac{V_0^2}{2 - (2l_0/\nu)\, w_1 + ((l_0/\nu)\, w_1)^2}, \\ R_{13} &= R_{11}, \\ R_{23} &= R_{22}, \\ R_{12} &= 0, \\ R_{33} &= R_{11} + R_{22}, \end{aligned}\right\} \tag{4.1}$$

where $\boldsymbol{w} = (w_1, w_2, w_3)$ is the large-scale field.

The validity of (4.1), as approximate expressions for the Reynolds stresses, is not limited to just small Reynolds numbers. Indeed, when the large-scale flow $\boldsymbol{w}$ becomes strong, as it will if an inverse cascade is present, the nonlinear self-advection of the small-scale field $\tilde{\boldsymbol{u}}$ becomes negligible compared to its advection by the large-scale flow.

From now on, we shall work with a specific model which has the potential of capturing, at least qualitatively, what we observed in the full three-dimensional simulation of §3, while permitting us to go much further in the study of the inverse cascade. The model describes only large-scale flow, the dynamics of which is assumed to satisfy the AKA equation (2.3) with Reynolds stresses given by (4.1). We note that (2.3) admits non-trivial one-dimensional solutions (as we shall see), but it also admits two- and three-dimensional solutions. In this paper we restrict ourselves to the former case, with some comments on the latter in the conclusion. Specifically, we assume spatial dependency only on the $z$-coordinate, which corresponds to the (linearly) most unstable modes.

Substituting (4.1) into (2.3) with only $z$-dependence, we obtain a system of PDEs henceforth referred to as the nonlinear AKA equation:

$$\left.\begin{aligned} \frac{\partial u}{\partial T}+\frac{\alpha}{2}\frac{\partial}{\partial Z}\left(\frac{1}{1+v+\frac{1}{2}v^2}\right) &= \frac{\partial^2 u}{\partial Z^2}, \\ \frac{\partial v}{\partial T}+\frac{\alpha}{2}\frac{\partial}{\partial Z}\left(\frac{1}{1-u+\frac{1}{2}u^2}\right) &= \frac{\partial^2 v}{\partial Z^2}. \end{aligned}\right\} \tag{4.2}$$

The variables used here are related to the original ones as follows:

$$\left.\begin{aligned} \alpha = R^2(L/l_0), \quad z = LZ, \quad t = (L^2/\nu)\,T, \\ u = R(w_1/V_0), \quad v = R(w_2/V_0), \end{aligned}\right\} \tag{4.3}$$

where $L$ characterizes the largest available scale in the flow.

Notice that, because the solution depends on $z$ only and the flow is incompressible, the nonlinear self-advection term in (4.2) drops out. Still, the modification of the Reynolds stresses by the large-scale flow results in a non-trivial 'feed-back' nonlinearity.

Hereafter we limit ourselves to solutions which are $2\pi$-periodic in the $Z$ variable. The only control parameter is then $\alpha$ given by (4.3). Although we assumed the forcing Reynolds number $R$ to be small, $\alpha$ also involves the aspect ratio $L/l_0$ and can thus be of arbitrary strength.

For $\alpha < 2$, the solution $u = v = 0$ is stable. As $\alpha$ crosses the value 2, the mode of wavenumber $k = 1$ becomes unstable, as readily seen by linearizing (4.2). At this point a steady subcritical bifurcation occurs (Frisch, She & Sulem 1988). Numerical integration of (4.2) near threshold, starting with small $u$ and $v$ has shown that, after transients, a finite amplitude steady solution is obtained.

Our main interest, in this paper, is in cases of large $\alpha$, when there is a wide range of unstable modes, a prerequisite for an inverse cascade. For such strongly nonlinear regimes, it is of interest to put (4.2) in a more symmetrical form:

$$\left.\begin{aligned} \frac{\partial U}{\partial T}+\alpha\frac{\partial}{\partial Z}\left(\frac{1}{1+V^2}\right) &= \frac{\partial^2 U}{\partial Z^2}, \\ \frac{\partial V}{\partial T}+\alpha\frac{\partial}{\partial Z}\left(\frac{1}{1+U^2}\right) &= \frac{\partial^2 V}{\partial Z^2}, \end{aligned}\right\} \tag{4.4}$$

where

$$U = u-1, \quad V = v+1. \tag{4.5}$$

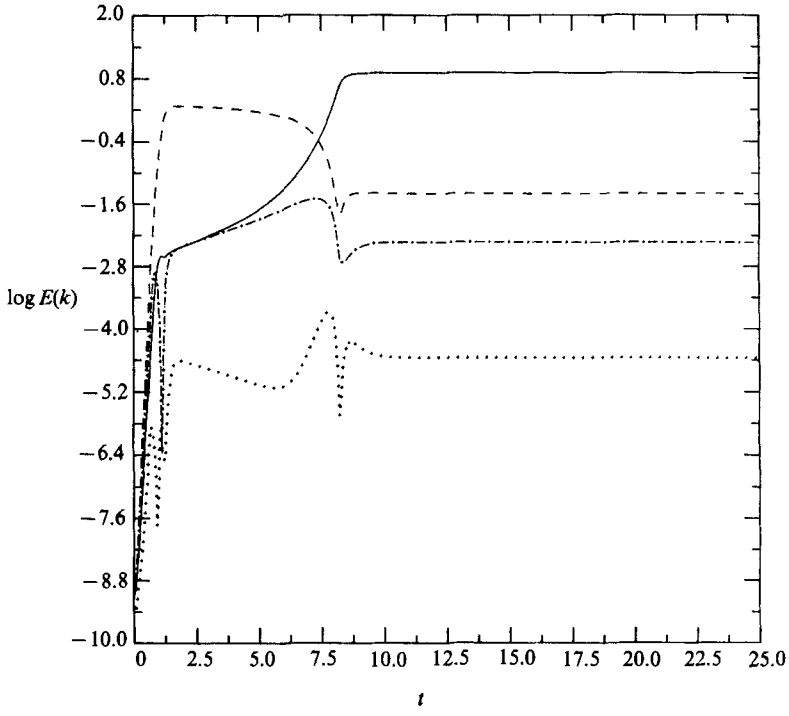


FIGURE 3. Simulation of the one-dimensional nonlinear AKA equation (4.4) governing the large-scale dynamics for $\alpha = 9$. The figure shows the evolution, in lin–log coordinates, of the energy $E(t, k)$ for $k = 1$ (full), $k = 2$ (dashed), $k = 3$ (dashed-dotted), and $k = 4$ (dotted). Note that the behaviour of modes $k = 1$ and $k = 2$ is similar to that of the full simulation (figure 1).

The simplification which occurs by this velocity shift is related to the fact that the stirring force (3.1) can be made time-independent via a Galilean transformation. In the $(u, v)$ variables, it is natural to impose the absence of any uniform component: $\bar{u} = \bar{v} = 0$, a condition which is preserved in time. Here, the overline bar denotes averaging over the $2\pi$ periodicity in the $Z$ variable. As a consequence,

$$\bar{U} = -1, \quad \bar{V} = +1. \tag{4.6}$$

We now report on a detailed numerical exploration of (4.4). The numerical scheme used is a collocation spectral method in space; the time marching is done by a 'slaved Adams–Bashforth' scheme, an adaptation of the 'slaved-frog' scheme (Frisch, She & Thual 1986). With suitable resolution (up to 3000 collocation points for $\alpha = 700$), this scheme provides the high accuracy required for large $\alpha$. Initial conditions had a low amplitude random excitation with a flat spectrum extending from $k = 1$ to $k = 8$.

Figure 3 shows the evolution of the energy of Fourier modes with $k$ from 1 to 4, for $\alpha = 9$. This is qualitatively quite similar to figure 1 obtained from the full three-dimensional simulation. In particular, the linearly most unstable mode, here $k = 2$, dominates at first. Then the mode $k = 1$ leap-frogs the mode $k = 2$ and finally a steady state is obtained. Thus, the early symptoms of an inverse cascade, as observed in the full simulation, are reproduced by the one-dimensional nonlinear AKA equation. By increasing considerably the number of unstable modes, we were able to observe an actual inverse cascade. Figures 4(*a*) and 4(*b*) correspond to $\alpha = 128$. They

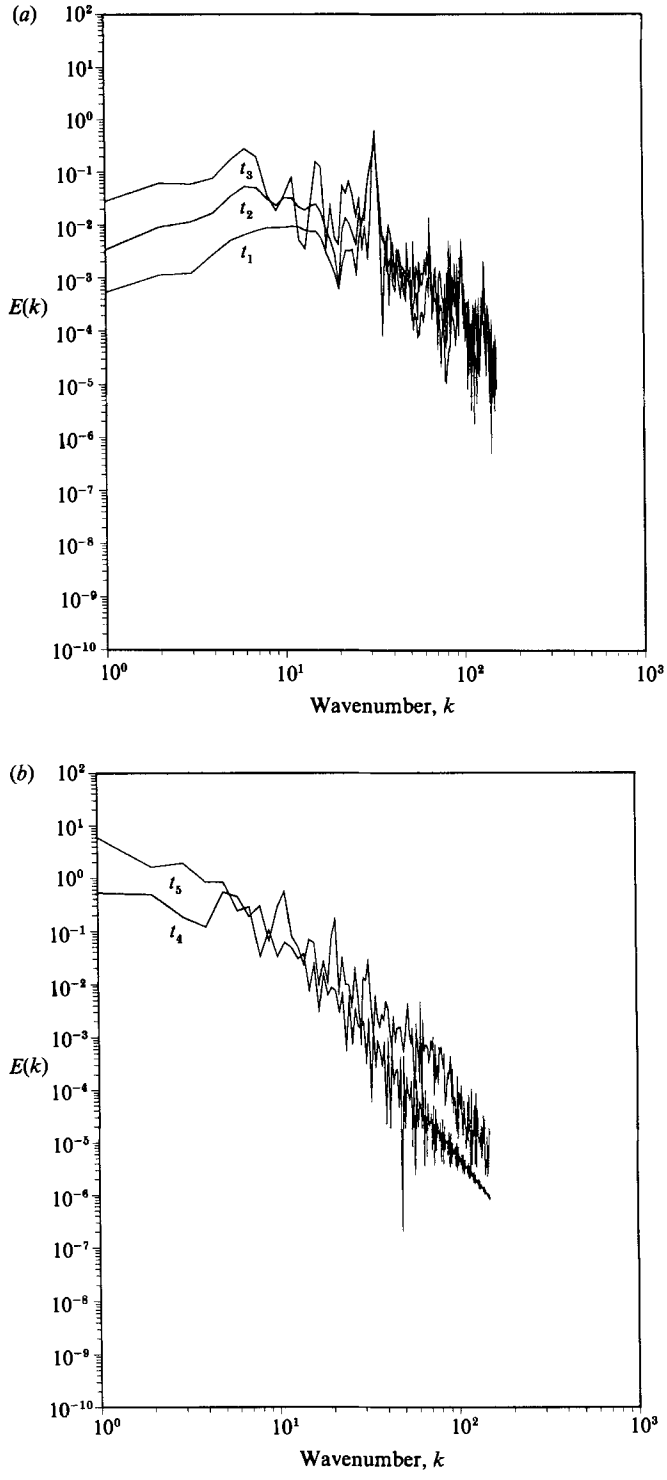


FIGURE 4. Simulation of an inverse cascade using the nonlinear AKA equation (4.4), for $\alpha = 128$. Log–log representation of the energy spectrum for (*a*) various early times and (*b*) later times. The labels $t_1$ to $t_5$ correspond to times $t = 0.02$, 0.04, 0.09, 0.23, 1.5, respectively. The latest time is in the steady state. For clarity, the spectra beyond $k = 150$, which fall off very quickly, are not shown.

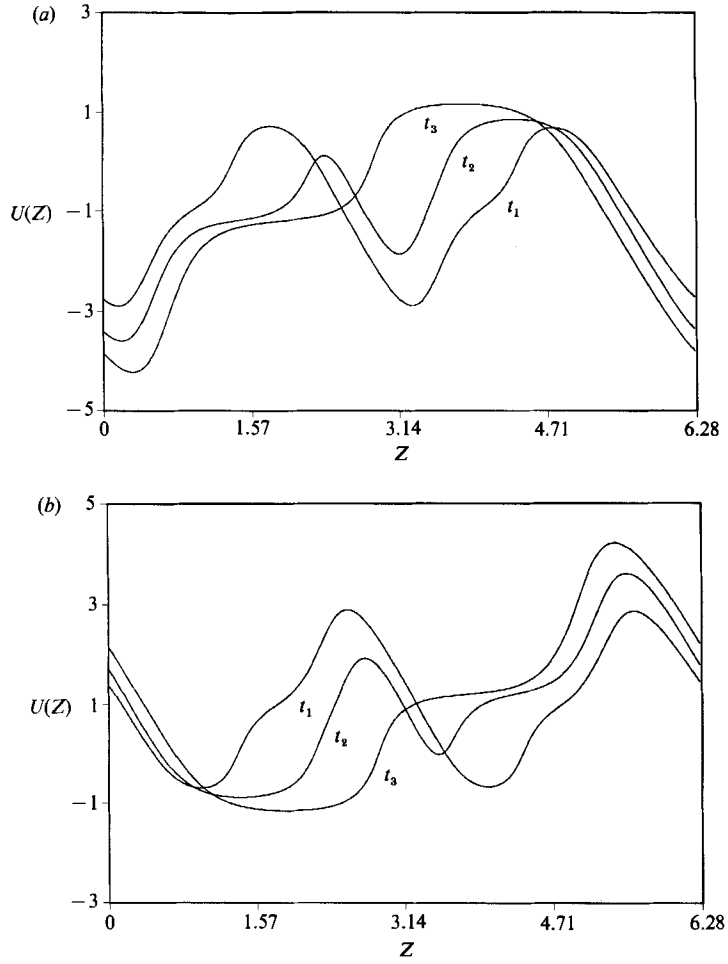


FIGURE 5. Evolution of the spatial structure of the solution to the nonlinear AKA equation for $\alpha = 9$ (*a*) $U(t, Z)$; (*b*) $V(t, Z)$). The labels $t_1$, $t_2$ and $t_3$ correspond to times $t = 1, 7, 10$. Note the transition from a two-hump to a one-hump solution. The latest time is in the steady state.

show the energy spectrum in log–log coordinates at various times. The energy spectrum is defined as $E(k) = \frac{1}{2}(|\hat{u}(k)|^2 + |\hat{v}(k)|^2)$, where $\hat{u}$ and $\hat{v}$ are the Fourier transforms of $u$ and $v$. We see that the energy grows, while migrating to smaller and smaller wavenumbers. Eventually, a steady state is obtained.

It is of interest to look at the evolution of the $(U, V)$ velocity field in the physical space. Figures 5(*a*) and 5(*b*) show $U(Z)$ and $V(Z)$, respectively, for $\alpha = 9$ at three times, chosen to correspond to interesting features in the evolution of the Fourier modes (figure 4). As long as the $k = 2$ mode dominates, we observe a two-hump solution; after the mode $k = 1$ leap-frogs the mode $k = 2$, we observe a one-hump solution, preserved into the steady state. We stress that in the process, a plateau is formed, where $U$ and $V$ are almost flat. This plateau gains considerable extension for higher values of $\alpha$ (see below).

Figures 6(*a*) and 6(*b*) show the evolution of the total energy $E = \frac{1}{2}\langle(u^2 + v^2)\rangle$ and the total helicity $H = \frac{1}{2}\langle(v\,\partial_Z u - u\,\partial_Z v)\rangle$ for different values of $\alpha$. The general trend in the energy is to increase in time for all values of $\alpha$, while the helicity has a more

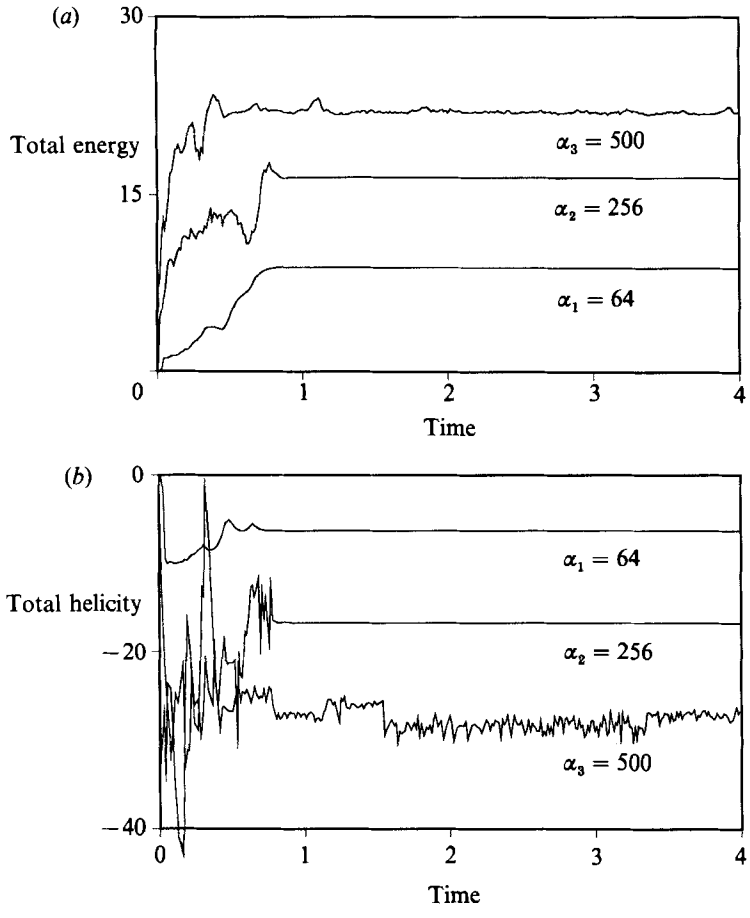


FIGURE 6. Evolution of (*a*) total energy and (*b*) total helicity for various values of $\alpha$.

complex behaviour. The resulting steady state has an energy growing with $\alpha$ and a negative helicity, which is also growing (in absolute value).

For all cases studied, we found that the solution locks eventually into a steady state. Figure 7 shows the steady state graphs of $U(Z)$ and $V(Z)$ for various values of $\alpha$. For all $\alpha$, the solutions are found to be antisymmetrical:

$$V(Z') = -U(-Z'), \quad Z' = Z - Z_0, \tag{4.7}$$

after a suitable shift $Z_0$. This antisymmetry is consistent both with the equations of motion (4.4) and the boundary conditions (4.6). For $\alpha \geqslant 8$, we observe that the solutions present plateaux of increasing extent. At the plateaux and in the narrow shock-like connecting structure, the solutions satisfy $U \approx V$, a symmetry consistent with (4.4), but not with (4.6). The latter condition is satisfied thanks to the presence of humps, which become increasingly narrow and high as $\alpha$ increases. Accurate numerical values for the heights of the plateaux and the humps are given in table 1. All digits shown are significant. Finally, in figure 8, we show the energy spectrum $E(k)$ for $\alpha = 600$. Oscillations, due to interference phenomena, are superimposed on a range following approximately a $k^{-4}$ law; this reflects the existence in physical space of quasi-discontinuities of the slope at the hump-edges. At high $k$ there is a well-resolved dissipation range.

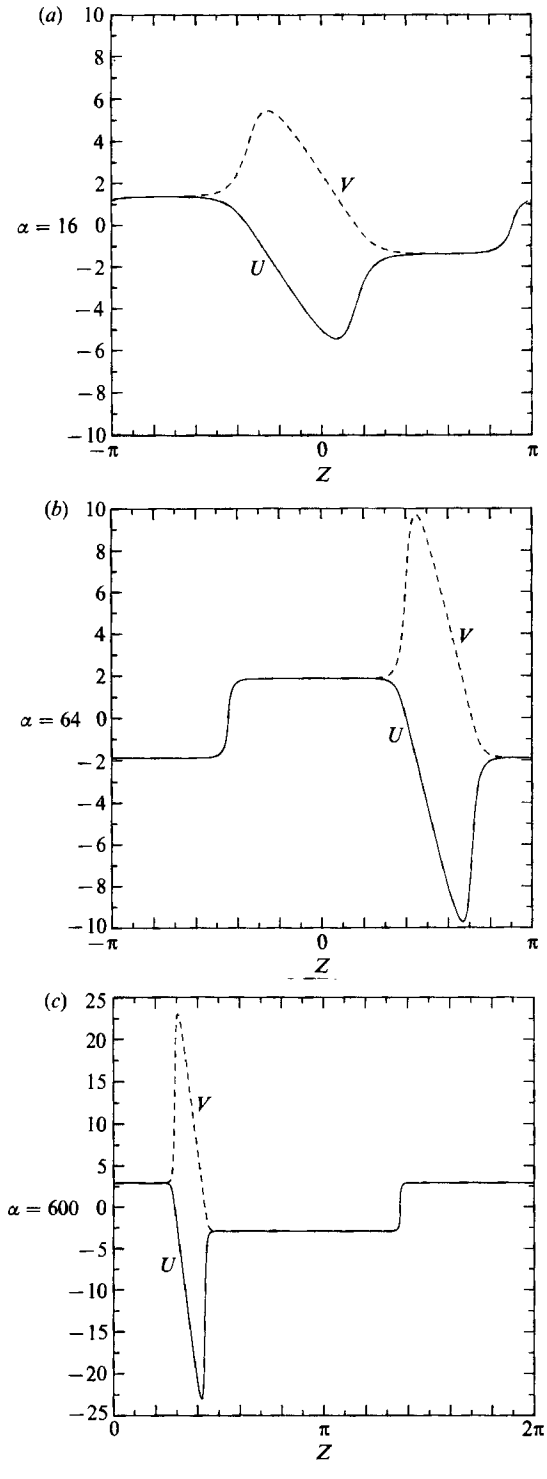


FIGURE 7. Steady state solutions to the nonlinear AKA equation for various values of $\alpha$. (*a*) 16; (*b*) 64; (*c*) 600. Note the increasingly sharp structures (plateaux, shocks, humps).

| $\alpha$ | $U_*$ | $M$ |
|---|---|---|
| 32 | 1.63 | 7.32 |
| 64 | 1.88 | 7.82 |
| 128 | 2.16 | 10.61 |
| 200 | 2.36 | 15.19 |
| 256 | 2.47 | 16.66 |
| 300 | 2.55 | 17.72 |
| 400 | 2.69 | 19.77 |
| 500 | 2.80 | 21.50 |
| 600 | 2.89 | 23.02 |
| 700 | 2.98 | 24.38 |

TABLE 1. Dependence on the control parameter $\alpha$ of the height of the plateaux $U_*$ and of the height of the hump $M$ for the steady state solution. All figures shown are significant.

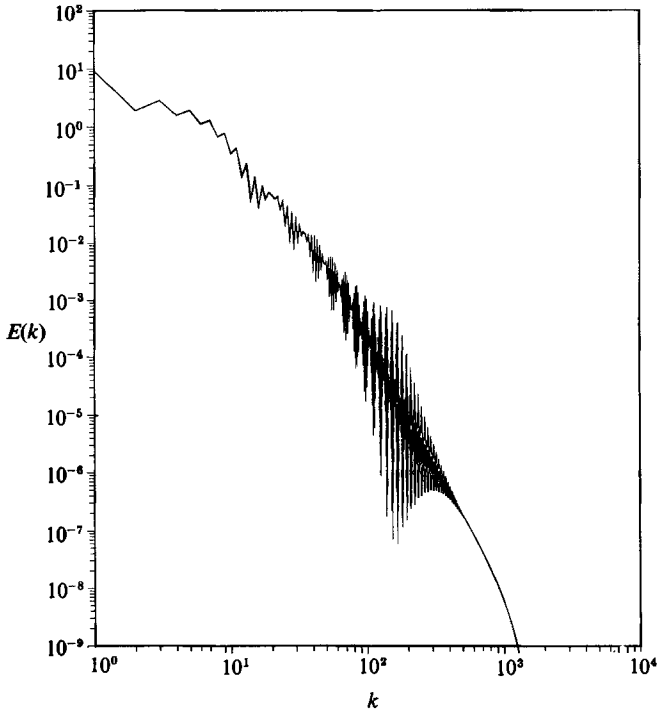


FIGURE 8. Steady state energy spectrum of the solution to the nonlinear AKA equation for $\alpha = 600$ in log–log coordinates. Note the power-law range (approximately $k^{-4}$) modified by oscillations due to interferences.

## 5. Scaling laws for the steady state

At this moment, we have only limited analytic grasp on the evolution to the steady state. The latter, however, can be described rather thoroughly, especially for large $\alpha$.

We start from the nonlinear AKA equation (4.4) with the integral constraint (4.6) and the antisymmetry condition (4.7). Integrating once with respect to $Z$, we find that $U(Z)$ and $V(Z)$ are solutions to the system of first-order ODEs:

$$\frac{\partial U}{\partial Z} = \alpha\left(\frac{1}{1+V^2} - A\right), \quad \frac{\partial V}{\partial Z} = \alpha\left(\frac{1}{1+U^2} - A\right). \tag{5.1}$$

The constant of integration $A$ is the same for both equations, since it can be written as an average over the $2\pi$ period of $1/(1+U^2)$ or of $1/(1+V^2)$, which are equal in view of (4.7). These quantities are the only non-vanishing components of the Reynolds stress tensor. $A$ will thus be called the mean Reynolds stress.

There is an explicit parametric representation of $U$, $V$ and $Z$ in terms of

$$s = A(V-U). \tag{5.2}$$

This is obtained by the following steps. Eliminating $Z$ between the two equations of (5.1) and integrating once, we obtain

$$\arctan V - \arctan U = \arctan\left(\frac{V-U}{1+UV}\right) = A(V-U)+\epsilon, \tag{5.3}$$

where $\epsilon$ is a constant of integration. Taking the tangent of (5.3) and using (5.2), we obtain

$$UV = -1+\frac{s}{A\tan(s+\epsilon)}. \tag{5.4}$$

From this and (5.2), we obtain

$$U = \frac{1}{2A}(-s\pm\Delta^{\frac{1}{2}}), \quad V = \frac{1}{2A}(+s\pm\Delta^{\frac{1}{2}}), \tag{5.5a,b}$$

where

$$\Delta = s^2-4A^2+\frac{4As}{\tan(s+\epsilon)}. \tag{5.6}$$

Taking the difference of the two equations in (5.1), we obtain after some easy manipulations:

$$\alpha\,\mathrm{d}Z = \pm\frac{1}{A}\frac{s\,\mathrm{d}s}{\Delta^{\frac{1}{2}}\sin^2(s+\epsilon)}. \tag{5.7}$$

By integrating (5.7), we complete the explicit parametric representation. We need two conditions to determine the two constants of integration $A$ and $\epsilon$ in terms of $\alpha$. One of them is (4.6), the condition that the average over the period of $U$ be minus one. The other one is that the periodicity in $Z$ be $2\pi$.

Let us now consider the phase diagram in the $(U, V)$-plane. The autonomous system (5.1) has, for fixed $A$, a family of cycles parametrized by $\epsilon$, given by (5.3). For large $\alpha$ the period will be $O(\alpha^{-1})$, except if the cycles are passing very close to the hyperbolic critical points of (5.1), which are located at

$$U = V = \pm U_*, \quad U_* = \left(\frac{1}{A}-1\right)^{\frac{1}{2}}. \tag{5.8}$$

How close the cycle gets to the critical points is controlled by how small $\epsilon$ is. We can now understand qualitatively the salient features of the steady solutions to the nonlinear AKA equation for large $\alpha$. Figure 9 shows the phase diagram of the solution for $\alpha = 600$. Let us momentarily think of $Z$ as a time. The solution spends most of the time near the critical points; this corresponds to the plateaux of figure 7. The straight segment connecting the two critical points along the line $U = V$ corresponds to the shock-like structure in figure 7. The large loop connecting the critical points corresponds to the humps in figure 7. The transitions from the loop to the straight segment are along trajectories connecting stable and unstable directions near the critical points. These are too close to the critical points to be resolved in figure 9.

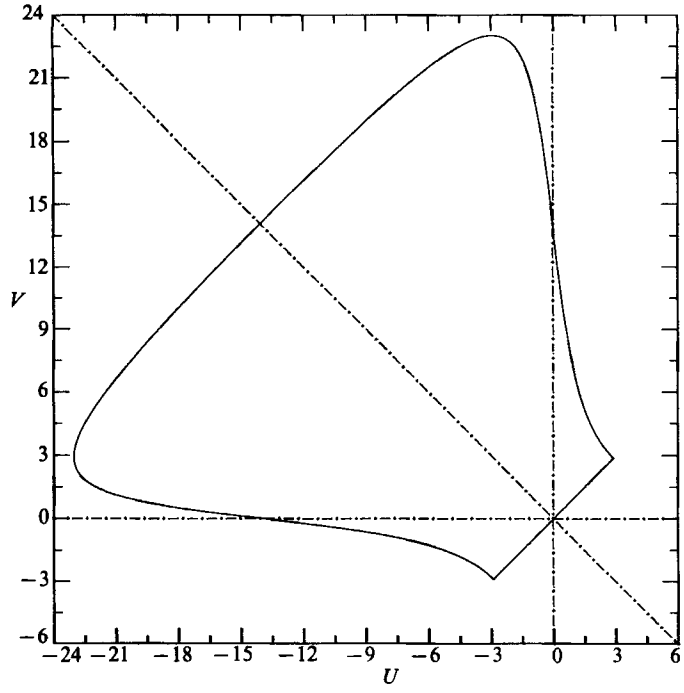


FIGURE 9. Phase-diagram in the $(U, V)$-plane of the steady solution to the nonlinear AKA equation for $\alpha = 600$.

We have measured the dependence of the two constants of integration $A$ and $\epsilon$ over a wide range of values of the control parameter $\alpha$ by numerical integration of the nonlinear AKA equation (4.4). The results are shown in table 2. It is seen that $A$ decreases to zero, but rather slowly, and that $\epsilon$ decreases very quickly. Their asymptotic behaviour, for large $\alpha$, can be obtained analytically as we now show.

We start from the parametric representation (5.5)–(5.7). In the $(U, V)$-plane, there is a symmetry with respect to the line $U+V=0$, corresponding to the plus and minus signs in front of $\Delta^{\frac{1}{2}}$. The condition of positivity of $\Delta$ defines the domain of variation of the parameter $s$. For small $A$ and $\epsilon$, the relevant roots of $\Delta$ are near 0 and $\pi$. They are easily found to be

$$s_m = \frac{\epsilon A}{1-A} + O(\epsilon^3 A), \quad s_M = \pi - \frac{4A}{\pi} + O(A^2) + O(\epsilon). \tag{5.9}$$

Since the origin for $Z$ has not yet been chosen, we can decide to have $Z=0$ correspond to $s = s_m$. Then, using the mentioned symmetry, we can restrict ourselves everywhere to the plus sign in front of $\Delta^{\frac{1}{2}}$, so that $Z = \pi$ corresponds to $s = s_M$. The two integral constraints, that the average of $V(Z)$ be one and that the half-period be $\pi$ are then expressed as

$$I = \int_0^{\pi} \mathrm{d}Z = \int_{s_m}^{s_M} \frac{1}{\alpha A} \frac{s\,\mathrm{d}s}{\Delta^{\frac{1}{2}} \sin^2(s+\epsilon)} = \pi, \tag{5.10}$$

and

$$J = \frac{1}{2\pi} \int_0^{2\pi} V(Z)\,\mathrm{d}Z = \frac{1}{2\pi} \int_{s_m}^{s_M} \frac{1}{\alpha A^2} \frac{s^2\,\mathrm{d}s}{\Delta^{\frac{1}{2}} \sin^2(s+\epsilon)} = 1. \tag{5.11}$$

In order to find $A$ and $\epsilon$ in terms of $\alpha$, we expand $I$ and $J$ for small $A$ and small $\epsilon$. For $J$ the main contribution is from the hump. For $I$ the main contribution is from

| $\alpha$ | $A$ | $\epsilon$ |
|---|---|---|
| 2 | 0.500012557 6 | 0.570746095 15 |
| 2.05 | 0.543754796 | 0.3732742 |
| 2.10 | 0.55239149 | 0.3218924 |
| 2.25 | 0.562642 7 | 0.2330350 |
| 2.5 | 0.563785 88 | 0.155074 |
| 3 | 0.550931 7 | 0.08597 |
| 6 | 0.461496 9 | 0.00448 |
| 8 | 0.423191 7 | 0.00094 |
| 9 | 0.408178 5 | 0.00045 |
| 16 | 0.341349 | — |
| 32 | 0.27441 | — |
| 64 | 0.22008 | — |
| 128 | 0.17617 | — |
| 200 | 0.15243 | — |
| 256 | 0.1408 | — |
| 300 | 0.13369 | — |
| 400 | 0.12174 | — |
| 500 | 0.11320 | — |
| 600 | 0.10669 | — |
| 700 | 0.10147 | — |

—, Too small to be computed

TABLE 2. Dependence on the control parameter $\alpha$ of the constants of integration $A$ and $\epsilon$. All figures shown are significant.

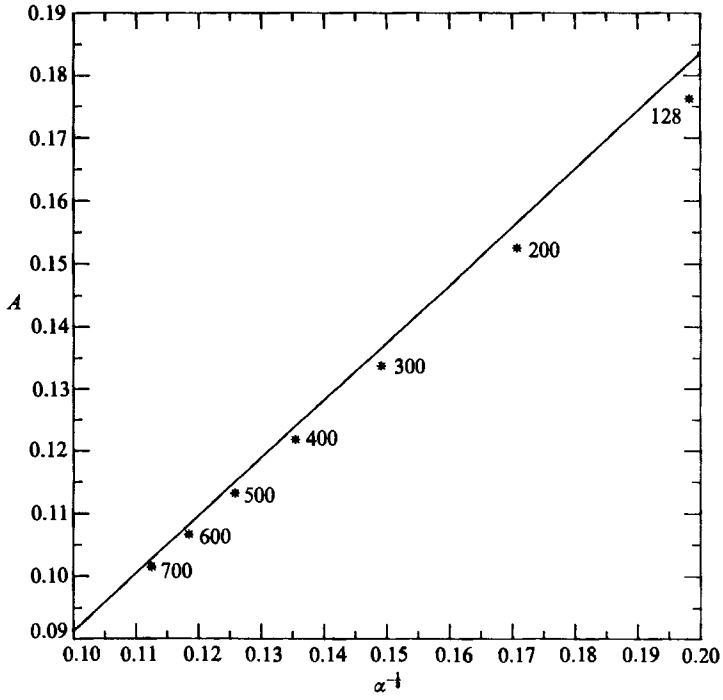


FIGURE 10. Comparison of the leading-order asymptotic prediction (full line) and numerically measured values for large $\alpha$. The mean Reynolds stress $A$, is plotted against $\alpha^{-\frac{1}{3}}$. The star symbols are labelled by the corresponding values of $\alpha$.

the neighbourhood of the critical points. The leading-order results for $\alpha \to \infty$ are given hereafter:

$$\alpha A^3 \sim \tfrac{1}{4}\pi, \tag{5.12}$$

$$\ln \epsilon \sim -\pi^{\frac{3}{2}}\alpha^{\frac{1}{2}}. \tag{5.13}$$

Figure 10 shows the measured values of the mean Reynolds stress $A$ plotted against $\alpha^{-\frac{1}{3}}$. There is good agreement with the leading-order asymptotics represented by the straight line. From (5.12) we also obtain the leading-order behaviour for $\alpha \to \infty$ of the heights of the plateaux $U_*$ and of the humps $M = \sup V(Z)$:

$$U_* \sim \alpha^{\frac{1}{3}}(\tfrac{1}{4}\pi)^{-\frac{1}{6}}, \tag{5.14}$$

$$M \sim \alpha^{\frac{1}{3}}(2\pi)^{\frac{2}{3}}. \tag{5.15}$$

## 6. Concluding remarks

We have found strong numerical evidence that small-scale forcing lacking isotropy and parity-invariance can lead to the formation of very energetic and helical large-scale structures. These are generated by a mechanism of inverse cascade with successive appearance of structures of larger and larger scales. Eventually, the flow goes to a steady-state dominated by structures of the largest available scale.

It has been noted by V. Arnold (private communication) that the very existence of such a steady state may be due to a feature of the steady state equations, (5.1), reflecting our special choice of forcing function. The flow in phase space defined by (5.1) has zero divergence. Since it is two-dimensional, it has generically closed orbits, i.e. space periodic solutions. The question of non-steady solutions with alternative forcing will be reported elsewhere.

Key features of the large-scale dynamics, as observed in the full three-dimensional simulations, are captured by an asymptotic expansion leading to the one-dimensional nonlinear AKA equations (4.4). From this equation, we obtained analytically the scaling laws for the steady-state solutions when the range of unstable modes becomes very wide.

It would be of interest to have a more analytic grasp of the time-evolution in the nonlinear regime governed by the nonlinear AKA equation (4.4). The steady equations possess 'cellular' solutions of period $2\pi/N$ for arbitrary integer $N$. The competition between these could play a role in the intermediate dynamics, as they clearly do in the Kolmogorov flow (She 1987).

So far, we limited out investigations to one-dimensional large-scale dynamics. This, however, was only to get some insight into the phenomena resulting from nonlinear feedback. The general case can be formulated as well. The relevant (multi-dimensional) nonlinear AKA equation is:

$$\partial_T w_i + \nabla_j(w_i w_j + R_{ij}(\boldsymbol{w})) = -\nabla_i p + \nu\nabla^2 w_i, \quad \nabla_j w_j = 0, \tag{6.1}$$

where

$$R_{ij} = \langle \tilde{u}_i \tilde{u}_j \rangle. \tag{6.2}$$

The small-scale field $\tilde{\boldsymbol{u}}$ is obtained from an equation with forcing and advection:

$$\partial_t \tilde{u}_i + w_j \partial_j \tilde{u}_i + \tilde{u}_j \partial_j \tilde{u}_i = f_i + \nu \partial_{jj}^2 \tilde{u}_i - \partial_i \tilde{p}, \quad \partial_j \tilde{u}_j = 0. \tag{6.3}$$

Note that $(\partial_T, \nabla)$ and $(\partial_t, \partial)$ refer to large and small scales respectively.

It is essential for the validity of the equations above that there be a separation of scales. As pointed out in §4, the required separation may be a consequence of a small Reynolds number, of a small anisotropy or of a weak parity-violation. In such

instances, the AKA instability is relegated to very large scales from the beginning. Alternatively, there may be a dynamical process of inverse cascade, the early stages of which are not described by equations (6.1)–(6.3), eventually leading to the build-up of a velocity field on scales much larger than the forcing. Such forcing may or may not lack parity-invariance and isotropy: in the nonlinear regime, this is irrelevant since full and not just linear dependence on $\boldsymbol{w}$ must be kept in the Reynolds stresses. Our equations (6.1)–(6.3) are then appropriate for the subsequent evolution. When there is an inverse cascade, we also expect the resulting velocity field to become strong, compared to the small-scale field. Further simplifications of the dynamics are then expected. The nonlinear self-advection term $\tilde{u}_j \partial_j \tilde{u}_i$ may then be dropped to leading order, so that (6.3) becomes effectively linear and may be solved explicitly. Furthermore, in case of large $\boldsymbol{w}$, the Reynolds stresses $R_{ij}$ will be small compared to $w_i w_j$. Still, in order to sustain the large-scale flow, the Reynolds stresses must remain relevant. This suggests that the large-scale flow emerging from such an inverse cascade should be an approximate solution of the Euler equations, except for boundary layers. When the large-scale flow is one-dimensional, this condition is trivially satisfied. In several space-dimensions, a large manifold of steady or unsteady large-scale flows with non-trivial geometry is permitted, such as vortices, Beltrami flows, etc.

The numerical calculations were done on the Cyber 180/990 of the Tel Aviv University and on the CRAY2 of the Centre de Calcul Vectoriel pour la Recherche (Palaiseau). Part of this work was done while one of us (U.F.) was a visiting 'supercomputer scientist' at Rutgers University. This work was supported by CEE grant ST-2J-0029-1-F and the National Science Foundation under Grant OCE-8716027.

## REFERENCES

André, J. C. & Lesieur, M. 1977 *J. Fluid Mech.* **81**, 187.

Brissaud, A., Frisch, U., Léorat, J., Lesieur, M. & Mazure, A. 1973 *Phys. Fluids* **16**, 1366.

Frisch, U., Léorat, J., Mazure, A. & Pouquet, A. 1975 *J. Fluid Mech.* **68**, 769.

Frisch, U., She, Z. S. & Sulem, P. L. 1987 *Physica* **28D**, 382.

Frisch, U., She, Z. S. & Sulem, P. L. 1988 In *Current Tendencies in Turbulent Research* (ed. H. Branover), Amer. Inst. Aeron. Astron. (In Press.)

Frisch, U., She, Z. S. & Thual, O. 1986 *J. Fluid Mech.* **168**, 221.

Kraichnan, R. H. 1967 *Phys. Fluids* **10**, 1417.

Kraichnan, R. H. 1976 *J. Atmos. Sci.* **33**, 1521.

Krause, F. & Rüdiger, G. 1974 *Astron. Nachr.* **295**, 93.

Meneguzzi, M., Frisch, U. & Pouquet, A. 1981 *Phys. Rev. Lett.* **47**, 1060.

Moffatt, H. K. 1978 *Magnetic Field Generation in Electrically Conducting Fluids.* Cambridge University Press.

Moiseev, S. S., Sagdeev, R. Z., Tur, A. V., Khomenko, G. A. & Yanovskii, V. V. 1983 *Z. Eksp. Teor. Fiz.* **85**, 1979; *Sov. Phys. J. Exp. Theor. Phys.* **58**, 1149.

She, Z. S. 1987 *Phys. Lett.* A **124**, 161.

Steenbeck, M., Krause, F. & Rädler, K. H. 1966 *Z. Naturforsch.* **21**, 369.